IEEE Photonics Journal
An IEEE Photonics Society Publication

Open Access

Broadband Extraordinary Optical Transmission Through Gold Diamond-Shaped Nanohole Arrays

Volume 6, Number 4, August 2014

Yong-Kai Wang
Yan Qin
Zhong-Yue Zhang

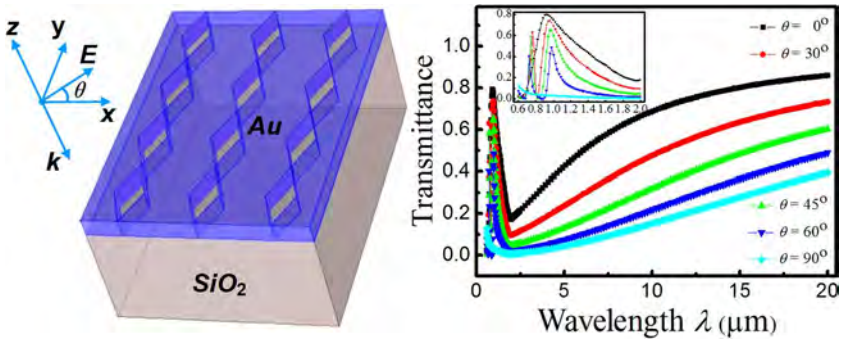

DOI: 10.1109/JPHOT.2014.2343153
1943-0655

IEEE photonics SOCIETY

IEEE

Broadband Extraordinary Optical Transmission Through Gold Diamond-Shaped Nanohole Arrays

Yong-Kai Wang,[1] Yan Qin,[2] and Zhong-Yue Zhang[1,2]

[1]School of Physics and Information Technology, Shaanxi Normal University, Xi'an 710062, China
[2]School of Physical Science and Technology, Southwest University, Chongqing 400715, China

DOI: 10.1109/JPHOT.2014.2343153

Manuscript received May 6, 2014; revised July 14, 2014; accepted July 18, 2014. Date of current version August 13, 2014. This work was supported in part by the National Natural Science Foundation of China under Grant 11004160 and in part by the Fundamental Research Funds for the Central Universities under Grant GK201303007. Corresponding author: Z. Zhang (e-mail: zyzhang@snnu.edu.cn).

Abstract: Extraordinary optical transmission (EOT) is widely accepted as a resonant phenomenon. However, the nonresonant EOT phenomenon of subwavelength metallic nanohole arrays on a metallic thin film is significant for harvesting of broadband light, confining optical power in small area, and enhancing local electric field. To achieve nonresonant EOT, a novel paradigm structure comprising periodic diamond-shaped nanohole arrays engraved on a thin gold film is proposed. The transmission properties of the diamond-shaped nanohole arrays are calculated using the finite-element method. Results show that this paradigm structure facilitates a broadband and enhanced transmission in the infrared region. In addition, the effects of incident polarization and structural parameters on the transmission property are also studied.

Index Terms: Extraordinary optical transmission, morphology dependent resonances, diamond-shaped nanohole arrays.

1. Introduction

In 1998, Ebbesen *et al.* studied the optical transmission of a metallic film perforated by an array of sub-wavelength holes. Results showed that surprisingly high transmission can be achieved for hole arrays, significantly exceeding the percentage of overall area covered with holes, although the diameter of a single isolated hole is considerably smaller than the wavelength of incident light. Such a phenomenon has been termed as extraordinary optical transmission (EOT) [1]. In addition to high transmittance, EOT also offers strongly enhanced localized field. Therefore, EOT has attracted considerable attention for its close association with sub-wavelength integrated optics [2], sensors [3], and nonlinear optical effects [4].

Numerous researchers have conducted remarkable investigations to explore the underlying physical mechanism behind EOT and then designed more efficient sub-wavelength nanohole structures with higher transmittance [5]–[20]. They found that RAs (sometimes referred to as a Wood anomaly or Rayleigh-Wood anomaly) play important roles in EOT [21], [22], which is associated with light diffracted parallel to the grating surface. RAs occur when

$$\frac{\omega}{c}\sqrt{\varepsilon_d} = |k_0 \sin\alpha + iG_x + jG_y|. \quad (1)$$

Here, $\omega, c, \varepsilon_d, k_0, \alpha, (i, j)$ are the angular frequency, light speed, the relative permittivity of the dielectric material, momentum of free-space light, the incident angle, and the order of specific RAs modes, respectively [23]. When light is incident on an array of sub-wavelength metallic holes with period constant a, photons can gain additional momentum in integer multiples of $|G_x| = |G_y| = 2\pi/a$. The wavelengths of the RAs occur at the onset of the (i, j) diffraction order, above which free-space light diffractions are forbidden. Resonant wavelength λ_{RA} decreases with the increased order of (i, j). Besides RAs, EOT is also influenced by surface plasmon polariton (SPP) on the surface of sub-wavelength metallic holes, which are generated under the Bragg coupling condition [23]

$$\mathrm{Re}\left[\frac{\omega}{c}\sqrt{\frac{\varepsilon_m \varepsilon_d}{\varepsilon_m + \varepsilon_d}}\right] = |k_0 \sin\alpha + iG_x + jG_y|. \tag{2}$$

Here, ε_m is the relative permittivity of the metal. Other parameters have the same meanings as those in (1). For metallic holes, localized surface plasmon (LSP) of the sub-wavelength metallic holes is also important to EOT. For example, an array of holes with acute angles was found to exhibit a strong EOT effect caused by the LSP [24]. Although RAs are nonresonant spectral feature, the interaction of RAs with SPPs or LSP on opposite sides of the metal film can lead to narrower spectral features and sometimes a higher EOT. Unlike the coupling between SPPs at two surfaces of metallic film, the coupling between RAs and SPPs or LSP only occurs for a range of film thicknesses [23]. Furthermore, Ruan *et al.* found that the localized waveguide resonances in the air hole also results in enhanced transmission, where the air hole can be considered as a section of metallic waveguide with both ends open to free space [8]. When the structure morphology of array holes is changed, the peaks, called morphology dependent resonances (MDR), are shifted in the transmission spectra [25]. It is manifested by the facts that metallic and non-metallic holes have the same EOT effect when their MDR of the hole are excited [26]. However, metallic holes can confine and enhance larger electric field on the surface of metallic holes.

The resonant phenomena caused primarily by MDR, SPP, LSP, and localized waveguide resonances in the EOT inevitably have a narrow spectral bandwidth. Limited control of the bandwidth can be achieved by engineering the interaction between resonances. However, studying broadband transparency is especially instructive and significant. Broadband transparency has recently been achieved using a nonresonant approach. For example, researchers obtained broadband EOT using oblique incidence transverse magnetic (TM) polarization [27], [28]. In addition, researchers found that larger rectangular apertures connected with smaller apertures [29], or metallic gratings with tapered slits [30] can also produce broadband EOT.

This study shows that diamond-shaped nanohole arrays operating under normal incidence can also generate broadband transmission for TM polarized light. The finite element simulation software COMSOL Multiphysics was used to study numerically the transmittance spectrum between the wavelength ranges of 0.6 μm to 20 μm. The simulation results show that the proposed structure not only possesses all the capabilities of EOT, but also achieves a nonresonant and broadband enhanced transmission in infrared. In addition, the transmission of light also depends on the morphology of the diamond-shaped nanohole. These results can be helpful for designing near-field light harvesting devices with broadband and strong transmission.

2. Structure and Computational Method

The schematic structure of the proposed diamond-shaped nanohole arrays is shown in Fig. 1. The diamond-shaped nanoholes are engraved on thin gold (Au) films with thickness d_{Au}. The Au film rests on top of a substrate with relative permittivity of $\varepsilon_d = 2.1025$ and thickness $d_{\mathrm{sub}} = 200$ nm. Except the discussion of the effect of the period on the transmission properties of the diamond-shaped nanorod arrays, the rectangular lattices of nanohole arrays in the x and y directions are $a = 200$ nm and $b = 200$ nm, respectively. The dimensions of the diamond-shaped

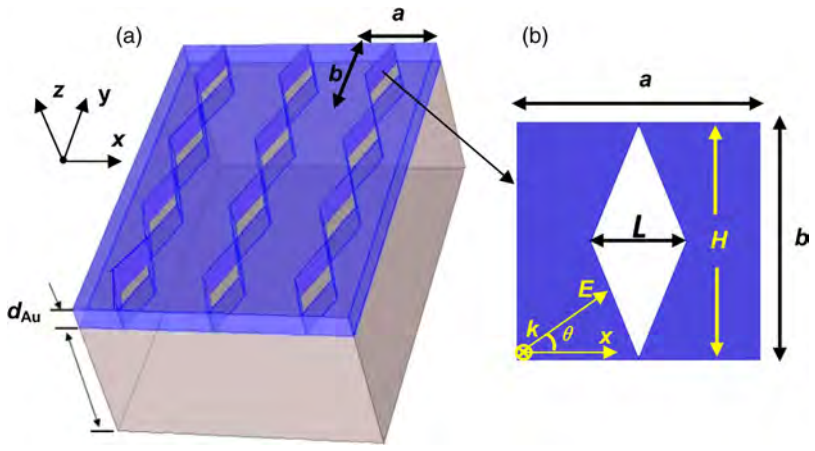

Fig. 1. (a) Proposed paradigm structure consisting of Au patterned film with thickness d_{Au} resting on a d_{sub} thick substrate. (b) The unit cell of the structure is magnified and depicted on the right panel (top view), with the associated geometric features.

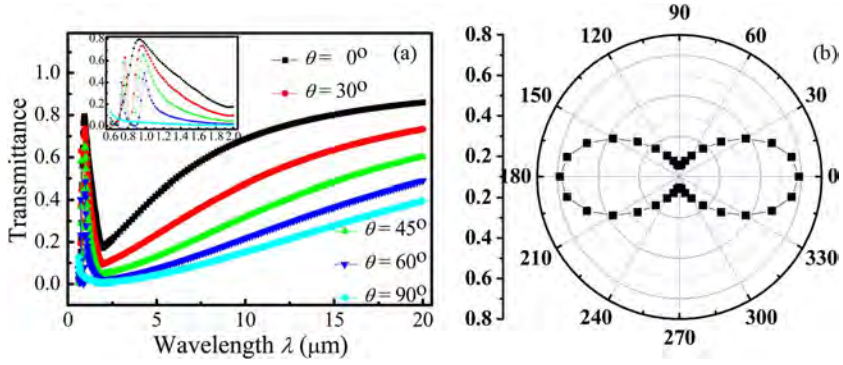

Fig. 2. (a) Transmission spectra of the diamond-shaped nanohole arrays irradiated by light with polarizations of $\theta = 0°$, 30°, 45°, 60°, 90°. Inset figure is the transmittance spectra of the wavelength ranging from 0.6 μm to 2.0 μm. (b) Polar plot of the transmittance of the diamond-shaped nanohole arrays at $\lambda = 10$ μm with different polarizations.

nanohole are shown in the right panel of Fig. 1. The diagonals of the diamond-shaped have a width L and a height H.

In this paper, the three-dimensional commercial FEM software COMSOL Multiphysics is used to simulate the transmission properties of the diamond-shaped nanohole arrays, where the frequency-dependent permittivities of Au are referred to Ref. [31]. In all calculations, light incident in the z direction with different polarization angles θ is shown in Fig. 1(b), where θ is defined as the angle with respect to the x-direction in the x–y plane.

3. Results and Discussion

Given the anisotropic structure of diamond-shaped nanohole arrays, light incident polarization would possibly affect their transmission property. To investigate how the polarization of the incident light influences the transmission properties of diamond-shaped nanohole arrays, the polarization angle θ is increased from 0° to 90° at fixed $L = 80$ nm, $H = 200$ nm, and $d_{Au} = 50$ nm as shown in Fig. 2(a). Inset figure in Fig. 2(a) shows the transmittance spectra of the wavelength ranging from 0.6 μm to 2.0 μm. When $\theta = 0°$, a broadband in the infrared and the high transmission peak of $\lambda \approx 0.96$ μm appear in the transmission spectrum. When $\theta = 30°$, new peaks appear around $\lambda \approx 0.745$ μm. With increased θ, the transmittances at the two peaks and the broadband decreased dramatically. When $\theta = 90°$, two peaks around $\lambda \approx 0.96$ μm and

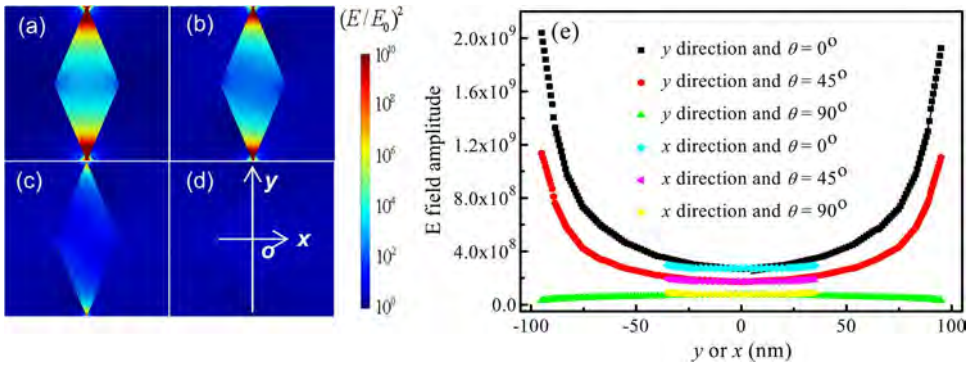

Fig. 3. (a)–(d) Contour profiles of the normalized $|E_z|$ fields of the diamond-shaped nanohole arrays at different polarizations at $\lambda = 10$ μm. (a) $\theta = 0°$. (b) $\theta = 30°$. (c) $\theta = 60°$. (d) $\theta = 90°$. (e) Electric field amplitude along the diagonal lines (x and y directions) under irradiations at $\lambda = 10$ μm with different polarization angles.

$\lambda \approx 0.745$ μm disappear in the transmittance spectrum of the wavelength ranging from 0.6 μm to 2.0 μm. Fig. 2(b) shows the polar plot of the transmittance at $\lambda = 10$ μm with different incident polarization angles. The maximum transmittance is found to occur at $\theta = 0°$ and $\theta = 180°$ and minimum transmittance at $\theta = 90°$ and $\theta = 270°$. Results show good agreement with those of previous studies [10]. For the arrays of sub-wavelength elliptical holes in a Au film, optical transmission strongly depends on the incident polarization, and maximum transmittance occurs when the incident polarization is perpendicular to the major axis of the elliptical hole [10].

From (1) and (2), when light is incident perpendicularly $(\alpha = 0°)$ and $(i, j) = (0, 1)$, RAs modes and SPPs modes occur in the transmittance spectra of the diamond-shaped nanohole arrays when

$$\lambda_{RA}(1,0) = P\sqrt{\varepsilon_d} \qquad \text{and} \tag{3}$$

$$\lambda_{spp}(1,0) = P\left(\text{Re}\left[\sqrt{\frac{\varepsilon_m \varepsilon_d}{\varepsilon_m + \varepsilon_d}}\right]\right). \tag{4}$$

According to the (3) and (4), λ_{RA} and λ_{SPP} increase as the increased period P. When $P = a = 200$ nm and $\varepsilon_d = 2.1025$ (for the glass substrate of the bottom surface of metal film), $\lambda_{RA} \leq 0.6$ μm. When $P = \text{a} = 200$ nm and $\varepsilon_d = 1$ (for air of the top surface of metal film), $\lambda_{SPP} \leq 0.6$ μm. And the transmittance peaks around $\lambda \approx 0.745$ μm and $\lambda \approx 0.96$ μm still appear when $d_{\text{sub}} = 0$ nm (not shown). Thus, the transmittance peaks around $\lambda \approx 0.745$ μm and $\lambda \approx 0.96$ μm are not due to the resonances of RAs or SPPs. To further understand the reason of peaks of $\lambda \approx 0.745$ μm and $\lambda \approx 0.96$ μm of diamond-shaped nanohole arrays, we also calculated the transmission spectra of nonmetal material Si diamond-shaped nanohole arrays at $\theta = 0°$, 30°, 45°, 60°, and 90°. There are no transmission peaks around $\lambda \approx 0.745$ μm and $\lambda \approx 0.96$ μm (not shown). Therefore, the peaks of $\lambda \approx 0.745$ μm and $\lambda \approx 0.96$ μm not only related with morphology but also film materials. Through simulating the electric field distributions at xy-plane (not shown), it is found that strong electric field enhancements all occur inside the corners with a smaller corner angle of the diamond-shaped in xy-plane. For the peaks around $\lambda \approx 0.96$ μm, electric field enhancement distributions are symmetrical due to electron oscillations along x-direction. When $\theta \neq 0°$, 90°, incident electric field is asymmetrical with the diamond-shaped nanoholes. For the peaks around $\lambda \approx 0.745$ μm, electric field distributions are asymmetrical and oblique due to electron oscillations along the direction from upper right to lower left.

The electric field spatial distributions (normalized by the incident field amplitude E_0) at $\lambda \approx 10$ μm were calculated to understand the polarization-dependent transmittance spectra, as shown in Fig. 3(a)–(d). The structural parameters are the same as those in Fig. 2. When $\theta = 0°$, strong electric field enhancements occur inside the corners with a smaller corner angle and weak electric field enhancements occur inside the corners with larger corner angle of the

diamond-shaped. With the increase in θ, both the electric field enhancements inside corners with smaller and larger corner angles decrease dramatically. Fig. 3(e) shows the electric field amplitude along the diagonal lines under irradiations with different polarization angles. As shown in Fig. 3(d), the diagonal lines locate at x- and y-directions, respectively. The length of the diagonal line in y-direction is longer than that of the diagonal line in x-direction. The origin of x and y locates at the center of the diamond-shaped nanohole. In Fig. 3(e), the curves ranging from ~ -95 nm to $\sim$95 nm denote the electric fields along the diagonal line in y-direction. The curves ranging from ~ -35 nm to $\sim$35 nm denote the electric fields along the diagonal line in x-direction. When $\theta = 0^\circ$ and 45°, there are strong electric fields distributed in the corners with smaller corner angle and weak electric fields distributed in the corners with larger corner angle. The larger electric field distribution would result in the stronger transmittance in Fig. 2(a). When light incident with the polarization is perpendicular to the longer axis of the diamond-shaped nanohole, the resonance in x-direction of the diamond-shaped nanohole is excited by more light at the smaller angle corner of the diamond-shaped, which results in the maximum transmission at $\theta = 0^\circ$. When $\theta = 90^\circ$, the electric fields along diagonal lines in x- and y-direction are weak than those at $\theta = 0^\circ$ and 45°, which results in smaller transmittance in Fig. 2(a). These highly enhanced electric fields in the small-gap area of the diamond-shaped would be useful for optofluidic devices and for the enhancement of nonlinear optical properties [4].

For the irradiation at $\theta = 0^\circ$, when the wavelength of incident light is much larger than the period of the diamond-shaped nanoholes in x-direction, electrons on metal film congregate to the corner with smaller corner angle. The formed the strong electron oscillations between the two sides of the thin slit promote the diffraction effect of nonresonant RAs. In Fig. 3(e), the black line that ranges from 0 nm to 95 nm is fitted by the equation, electric field amplitude $E = 3.39 \times 10^{10}/(106.8. - y)$. It shows that electric fields distributed in the corners with small corner angle stronger than larger corner angle. Correspondingly, the width of diamond-shaped nanohole in x-direction $w = 0.8 * (100 - y)$. Because $w^* E \approx$ constant, the fitting results denote that there are same potential differences across the diamond-shaped nanoholes. Larger electric fields occur around the small corner of the diamond-shaped nanoholes and smaller electric fields occur around the large corner. The excited energy on the film is confined in small area and more easily goes through the diamond-shaped nanoholes from the small corner, which is consistent with previous results of [29].

When $H = L = 200$ nm, the diamond-shaped nanoholes are connected in both x- and y-direction $(a = b = 200$ nm), resulting in the same transmittance spectra at x-direction polarization incidence and y-direction polarization incidence. Because any incident polarization can be decomposed into two cases of x-direction and y-direction, the transmittance spectra of diamond-shaped nanohole arrays at $H = L = 200$ nm are incident polarization independent.

To investigate how the width L of the diamond-shaped nanohole affects the transmittance spectrum, L is increased from 40 nm to 200 nm at fixed $\theta = 0^\circ$, $H = 200$ nm, and $d_{Au} = 50$ nm. As shown in Fig. 4, the resonant transmission peaks slightly blue shift due to the decreasing of the electric oscillation distance in x-direction on metal film as L increases. The evident increase of the transmittances at the resonant peak and the nonresonant broadband could be attributed to the increase of area ratio of the nanoholes to the entire surface. As shown in Fig. 3(a), when $\theta = 0^\circ$, larger transmittances are attributed to the electron resonance in x-direction near the tips of the smaller corner angle. More electrons are blocked by the diamond-shaped and consequently turn to the tips of the smaller corner angle of the diamond-shaped nanohole with the increase of L, which enhances the electric field distribution in the corners with small corner angle of the diamond-shaped nanohole.

In addition, to investigate how the height H of the diamond-shaped cavity affects the transmittance spectrum, H is increased from 40 nm to 200 nm at fixed $L = 80$ nm, $\theta = 0^\circ$, and $d_{Au} = 50$ nm. In all calculations, the rectangular lattice in the y direction is fixed at $b = 200$ nm. Thus, the adjacent diamond-shaped nanoholes are connected at the tips of the smaller corner angle when $H = 200$ nm, and the adjacent diamond-shaped nanoholes are disconnected when $H < 200$ nm. As shown in Fig. 5, when H is decreased from 200 nm to 160 nm, the distance

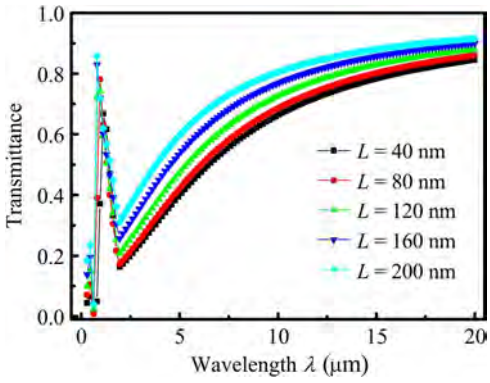

Fig. 4. Transmission spectra of the diamond-shaped nanohole arrays with different *L*.

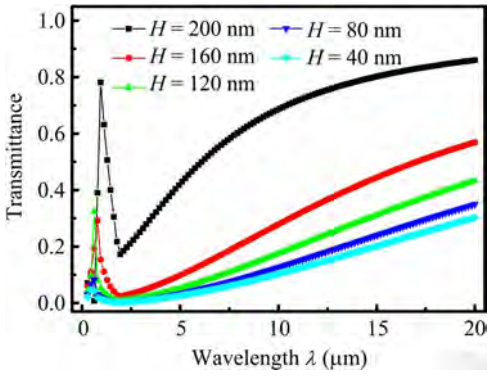

Fig. 5. Transmission spectra of the diamond-shaped nanohole arrays with different *H*.

between the tips of the smaller corner angle increased from 0 nm to 40 nm. Moreover, the transmittance at the peak and the broadband decreased dramatically as *H* decreases. Particularly, the maximum transmission of the diamond-shaped nanoholes is almost the same as through a thin gold film without apertures when $H <= 120$ nm. As discussed previously, at $\theta = 0^\circ$, the EOT of diamond-shaped nanohole arrays can be attributed to the electrons resonance in x-direction at $\lambda \approx 0.96$ μm and nonresonant RAs on the film at infrared. When *H* is less than 200 nm, the adjacent diamond-shaped nanoholes are disconnected. More electrons easily pass through the space between two adjacent diamond-shaped nanoholes, which result in decreased transmittance as *H* decreases.

Furthermore, to investigate the effect of the thickness d_{Au} of the diamond-shaped nanohole on the transmittance spectrum, d_{Au} is increased from 30 nm to 70 nm, with fixed $\theta = 0^\circ$, $L = 80$ nm, and $H = 200$ nm. As shown in Fig. 6, the transmission peak around 0.96 μm slightly blue shift with the increase of d_{Au}, which is due to the decrease of the ratio of the dimension in *x*-direction to *z*-direction. It is equivalent to the decreasing of the electric resonant distance in *x*-direction on metal film which is consistent with our previous conclusion that the peak is dependent on electric resonance in *x*-direction. In addition, with the increase of d_{Au}, the transmittance obviously decreases at broadband region, which is due to the increase of the loss in the propagation with the increase of d_{Au}.

Finally, to investigate the effect of the period *a* of the diamond-shaped nanohole on the transmittance spectrum, *a* is increased from 200 nm to 400 nm, with fixed $\theta = 0^\circ$, $L = 80$ nm, $H = 200$ nm, and $d_{Au} = 50$ nm. As shown in Fig. 7, the transmission peak around 0.96 μm slightly red shift with the increase of *a*, which is due to the increasing of the electric resonant distance in *x*-direction on metal film as an increases. With the increase of *a*, the transmittance

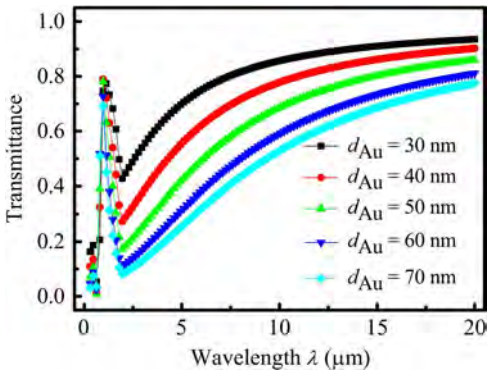

Fig. 6. Transmission spectra of the diamond-shaped nanohole arrays with different d_{Au}.

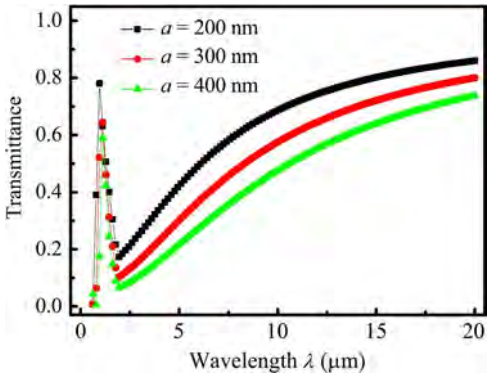

Fig. 7. Transmission spectra of the diamond-shaped nanohole arrays with different *a*.

obviously decreases at broadband region, which is due to the increase of the loss in the electron propagation with the increase of *a*.

4. Conclusion

In this study, a novel paradigm structure of diamond-shaped nanohole arrays is proposed to realize nonresonant and broadband EOT. The transmittance spectra and the normalized electric field distribution of the diamond-shaped nanohole arrays are investigated using the finite element method. Results show that the transmission properties of the diamond-shaped nanohole arrays strongly depend on incident polarization. Enhanced and broadband optical transmission can be achieved when light incident with the polarization is perpendicular to the diamond-shaped chains. In addition, the structural parameters of the diamond-shaped strongly affect the transmittance properties. The demonstrated capabilities of the proposed structure can be important for broadband light harvesting and nonlinear optical effect enhancement.

References

[1] T. W. Ebbesen, H. J. Lezec, H. F. Ghaemi, T. Thio, and P. A. Wolff, "Extraordinary optical transmission through sub-wavelength hole arrays," *Nature*, vol. 391, no. 6668, pp. 667–669, Feb. 1998.
[2] W. L. Barnes, A. Dereux, and T. W. Ebbesen, "Surface plasmon subwavelength optics," *Nature*, vol. 424, no. 6950, pp. 824–830, Aug. 2003.
[3] M. Das *et al.*, "Improved performance of nanohole surface plasmon resonance sensors by the integrated response method," *IEEE Photon. J.*, vol. 3, no. 3, pp. 441–449, Jun. 2011.

[4] Z. Q. Tian, B. Ren, and D. Y. Wu, "Surface-enhanced Raman scattering: From noble to transition metals and from rough surfaces to ordered nanostructures," *J. Phys. Chem. B*, vol. 106, no. 37, pp. 9463–9483, Sep. 2002.
[5] A. Degiron, H. J. Lezec, W. L. Barnes, and T. W. Ebbesen, "Effects of hole depth on enhanced light transmission through subwavelength hole arrays," *Appl. Phys. Lett.*, vol. 81, no. 23, pp. 4327–4329, Dec. 2002.
[6] A. Degiron and T. W. Ebbesen, "The role of localized surface plasmon modes in the enhanced transmission of periodic subwavelength apertures," *J. Opt. A, Pure Appl. Opt.*, vol. 7, no. 2, pp. S90–S96, Feb. 2005.
[7] K. J. Klein Koerkamp, S. Enoch, F. B. Segerink, N. F. van Hulst, and L. Kuipers, "Strong influence of hole shape on extraordinary transmission through periodic arrays of subwavelength holes," *Phys. Rev. Lett.*, vol. 92, no. 18, pp. 183 9011–183 9014, May 2004.
[8] Z. C. Ruan and M. Qiu, "Enhanced transmission through periodic arrays of subwavelength holes: The role of localized waveguide resonances," *Phys. Rev. Lett.*, vol. 96, no. 23, pp. 233901-1–233901-4, Jun. 2006.
[9] H. T. Liu and P. Lalanne, "Microscopic theory of the extraordinary optical transmission," *Nature*, vol. 452, no. 7188, pp. 728–731, Apr. 2008.
[10] R. Gordon *et al.*, "Strong polarization in the optical transmission through elliptical nanohole arrays," *Phys. Rev. Lett.*, vol. 92, no. 3, pp. 037401-1–037401-4, Jan. 2004.
[11] F. J. Garcia-Vidal, E. Moreno, J. A. Porto, and L. Martin-Moreno, "Transmission of light through a single rectangular hole," *Phys. Rev. Lett.*, vol. 95, no. 10, pp. 103901-1–103901-4, Sep. 2005.
[12] S. M. Orbons and A. Roberts, "Resonance and extraordinary transmission in annular aperture arrays," *Opt. Exp.*, vol. 14, no. 26, pp. 12 623–12 628, Dec. 2006.
[13] A. Mary, S. G. Rodrigo, L. Martin-Moreno, and F. J. Garcia-Vidal, "Theory of light transmission through an array of rectangular holes," *Phys. Rev. B*, vol. 76, no. 19, pp. 195414-1–195414-5, Nov. 2007.
[14] S. Wu, Q. J. Wang, X. G. Yin, J. Q. Li, and D. Zhu, "Enhanced optical transmission: Role of the localized surface Plasmon," *Appl. Phys. Lett.*, vol. 93, no. 10, pp. 101113-1–101113-3, Sep. 2008.
[15] Y. J. Bao *et al.*, "Role of interference between localized and propagating surface waves on the extraordinary optical transmission through a subwavelength-aperture array," *Phys. Rev. Lett.*, vol. 101, no. 8, pp. 087401-1–087401-1, Aug. 2008.
[16] C. L. Wang, J. Q. Gu, J. G. Han, Q. Xing, and Z. Tian, "Role of mode coupling on transmission properties of subwavelength composite hole-patch structures," *Appl. Phys. Lett.*, vol. 96, no. 25, pp. 251102-1–251102-3, Jun. 2010.
[17] Y. Ding, J. Yoon, M. H. Javed, S. H. Song, and R. Magnusson, "Mapping surface-plasmon polaritons and cavity modes in extraordinary optical transmission," *IEEE Photon. J.*, vol. 3, no. 3, pp. 365–374, Jun. 2011.
[18] R. Marani *et al.*, "Enhancement of extraordinary optical transmission in a double heterostructure plasmonic bandgap cavity," *Plasmonics*, vol. 6, no. 3, pp. 469–476, Sep. 2011.
[19] Y. M. Hou, "Extremely high transmittance at visible wavelength induced by magnetic resonance," *Plasmonics*, vol. 6, no. 2, pp. 289–293, Jun. 2011.
[20] G. H. Rui, Q. W. Zhan, and H. Ming, "Nanoantenna-assisted extraordinary optical transmission under radial polarization illumination," *Plasmonics*, vol. 6, no. 3, pp. 521–525, Sep. 2011.
[21] N. Garcia and M. Nieto-Vesperinas, "Theory of electromagnetic wave transmission through metallic gratings of subwavelength slits," *J. Opt. A: Pure Appl. Opt.*, vol. 9, no. 5, pp. 490–495, Mar. 2007.
[22] W. L. Barnes, W. A. Murray, J. Dintinger, E. Devaux, and T. W. Ebbesen, "Surface plasmon polaritons and their role in the enhanced transmission of light through periodic arrays of subwavelength holes in a metal film," *Phys. Rev. Lett.*, vol. 92, no. 10, pp. 107401-1–107401-4, Mar. 2004.
[23] J. M. McMahon, J. Henzie, T. W. Odom, G. C. Schatz, and S. K. Gray, "Tailoring the sensing capabilities of nanohole arrays in gold films with Rayleigh anomaly surface plasmon polaritons," *Opt. Exp.*, vol. 15, no. 26, pp. 18 119–18 129, Dec. 2007.
[24] S. G. Rodrigo *et al.*, "Holes with very acute angles: A new paradigm of extraordinary optical transmission through strongly localized modes," *Opt. Exp.*, vol. 18, no. 23, pp. 23 691–23 697, Nov. 2010.
[25] H. J. Lezec and T. Thio, "Diffracted evanescent wave model for enhanced and suppressed optical transmission through subwavelength hole arrays," *Opt. Exp.*, vol. 12, no. 16, pp. 3629–3651, Aug. 2004.
[26] N. Garcia and M. Bai, "Theory of transmission of light by sub-wavelength cylindrical holes in metallic films," *Opt. Exp.*, vol. 14, no. 21, pp. 10 028–10 042, Oct. 2006.
[27] X. R. Huang, R. W. Peng, and R. H. Fan, "Making metals transparent for white light by spoof surface plasmons," *Phys. Rev. Lett.*, vol. 105, no. 24, pp. 243901-1–243901-4, Dec. 2010.
[28] A. Alù, G. D'Aguanno, N. Mattiucci, and M. J. Bloemer, "Plasmonic Brewster angle: Broadband extraordinary transmission through optical gratings," *Phys. Rev. Lett.*, vol. 106, no. 12, pp. 123902-1–123902-4, Mar. 2011.
[29] G. Subramania, S. Foteinopoulou, and I. Brener, "Nonresonant broadband funneling of light via ultrasubwavelength channels," *Phys. Rev. Lett.*, vol. 107, no. 16, pp. 163902-1–163902-5, Oct. 2011.
[30] H. H. Shen and B. Maes, "Enhanced optical transmission through tapered metallic grating," *Appl. Phys. Lett.*, vol. 100, no. 24, pp. 241104-1–241104-3, Jun. 2012.
[31] P. B. Johnson and R. W. Christy, "Optical constants of the noble metals," *Phys. Rev. B*, vol. 6, no. 12, pp. 4370–4379, Dec. 1972.